Tellus (1980), *32*, 393–409

Non-linear, low order interactions

By E. KÄLLÉN[1] and A. C. WIIN-NIELSEN,[2] *European Centre for Medium Range Weather Forecasts, Shinfield Park, Reading, Berkshire RG2 9AX, U.K.*

(Manuscript received November 19, 1979; in final form February 5, 1980)

ABSTRACT

A study of the advection equation with Newtonian forcing and dissipation is presented. Only a few components in a spectral expansion of the simple advection equation are retained, and no rotation is included. Without forcing and dissipation the equation is thus only energy conserving.

A two component system is analysed in detail with respect to the number of steady states, their stability and the non-linear behaviour around the steady states. Depending on the forcing we obtain one or three steady states and their stability properties are forcing dependent. For some forcing values an unstable limit cycle develops around one of the steady states.

For a three component system the properties mentioned above are investigated for the conservative case and for the forced and dissipative case. Forcing on the largest scale, only, gives rise to one stable steady state. A more complicated behaviour is obtained when forcing is introduced on the smaller scales. Stable limit cycles may develop, as well as "catastrophes", i.e. a sudden change of the number of steady states for only a small parameter variation.

Generalizations from the behaviour of these simple systems to that of the atmosphere are difficult if not impossible. It is nevertheless believed that an analysis such as the one presented here may increase our understanding of the behaviour of multi-component systems.

1. Introduction

During recent years there has been a renewed interest in the non-linear behaviour of simple fluid dynamic systems. Low order spectral models of atmospheric flows have been used by Lorenz (1960) to obtain a maximum simplification of atmospheric models, and these models have been used to study specific behaviours in fluid systems such as the transition from Hadley to Rossby regimes in rotating flows (Lorenz, 1962). The same type of model has also been useful in studying some basic aspects of stochastic-dynamic predictions (Epstein, 1969; Fleming, 1971a,b; Pitcher, 1974) as well as the asymptotic behaviour of such systems (Wiin-Nielsen, 1976; 1979b). Most recently, low order systems with forcing and dissipation have been used by Charney and DeVore (1979), Vickroy and Dutton (1979) and Wiin-Nielsen (1979a) to determine the multiple steady states and their stability to suggest mechanisms for the establishment of certain stable flow regimes such as blocking.

The importance of non-linear processes in atmospheric flow through interactions among various scales has been well documented by several studies using atmospheric data (Yang, 1967; Saltzman, 1970; Steinberg et al., 1971; Chen and Wiin-Nielsen, 1978). These studies confirm the theoretical deductions by Fjørtoft (1953).

In this paper we will study a highly simplified version of the atmospheric equations of motion. The governing equation includes only one dimensional advection of wind and 'simple forcing and dissipation. From a meteorological point of view it would be more realistic to study the quasi-geostrophic, barotropic vorticity equation as was done by Lorenz (1960) and Vickroy and Dutton (1979). Our main object, however, is to investigate the advective non-linearity present in the equations governing atmospheric flow in its simplest form.

[1] On leave from Department of Meteorology, University of Stockholm, Arrhenius Laboratory, S-10691 Stockholm, Sweden.

[2] Present affiliation: World Meteorological Organization, Case Postale No 5, CH-1211, Geneva 20, Switzerland.

0040-2826/80/050393-17$02.50/0

The simplest equation containing this non-linearity is the scalar advective equation. Platzman (1964) discussed how the advective equation could be solved analytically and by an expansion in the spectral domain, but he did not include dissipation and forcing. Our study will concentrate on how the interplay between dissipation, forcing and advective non-linearities can give rise to a very interesting behaviour of the solutions. In order to make an analytical treatment tractable, we will work only with a spectral representation containing two or three components. The steady states, their stability and the asymptotic behaviour of trajectories as time goes to infinity will be investigated as functions of the scale and intensity of the forcing. A first attempt at such an analysis was made by Wiin-Nielsen (1975). The present paper is a continuation of that study.

2. A two component model

The basic equation is the advective equation with forcing and dissipation, i.e.

$$\frac{\partial u_*}{\partial t_*} + u_* \frac{\partial u_*}{\partial x_*} = -\varepsilon u_* + B(u_{E^*} - u_*) \tag{2.1}$$

Without forcing and dissipation this equation is energy but not enstrophy conserving.

After the following non-dimensionalization

$$u = \frac{\pi}{L(\varepsilon + B)} u_*$$

$$t = (\varepsilon + B) t_*$$

$$\xi = \frac{\pi}{L} x_*$$

$$u_E = \frac{\pi B}{L(\varepsilon + B)^2} u_{E^*},$$

where L is the lengthscale, equation (2.1) takes the form

$$\frac{\partial u}{\partial t} + u \frac{\partial u}{\partial \xi} = -u + u_E \tag{2.2}$$

Consider a distance $0 < \xi < \pi$ and define the boundary values by setting $u = 0$ for $\xi = 0$ and $\xi = \pi$. An expansion in the spectral domain can now be made with sinefunctions, only giving

$$u = \sum_{k=1}^{N} u(k) \sin k\xi,$$

$$u_E = \sum_{k=1}^{N} u_E(k) \sin k\xi$$

Inserting these expansions in (2.2) and reducing it to a two-component system we have the equations

$$\begin{aligned} \frac{dx}{dt} &= \tfrac{1}{2}xy - x + x_E \\ \frac{dy}{dt} &= -\tfrac{1}{2}x^2 - y + y_E \end{aligned} \tag{2.3}$$

where $u(1) = x$, $u(2) = y$, $u_E(1) = x_E$ and $u_E(2) = y_E$. Non-trivial interactions in the two-component system are possible, because the basic system has only one conservative property.

The first problem is to find the steady states, i.e. those states where $dx/dt = dy/dt = 0$. Denoting a steady state by (x_s, y_s) we find that all steady states are solutions to the equations

$$\begin{aligned} \tfrac{1}{2}x_s(y_s - 2) + x_E &= 0 \\ -\tfrac{1}{2}x_s^2 - y_s + y_E &= 0 \end{aligned} \tag{2.4}$$

leading to the equation

$$x_s^3 - 2(y_E - 2)x_s - 4x_E = 0 \tag{2.5}$$

The equations (2.4) may be considered as curves in the (x_s, y_s) plane. The steady states are given by the intersections of these curves. The parabola in Fig. 1 represents the curve $dy/dt = 0$, while the hyperbola corresponds to $dx/dt = 0$. The value of y_E determines the maximum of the parabola while x_E determines the shape of the hyperbola. It is thus seen that when y_E is smaller than a certain critical value there is only one intersection between the curves, i.e. one steady state. Three intersections (three steady states) will exist when y_E is larger than the critical value. The critical value is dependent on x_E and we must thus investigate the number of real roots in (2.5). They are determined by the quantity

$$\Delta = 4(x_E^2 - \tfrac{2}{27}(y_E - 2)^3) \tag{2.6}$$

according to the classical theory of the cubic equation. When $\Delta < 0$ we have three real roots. For $\Delta > 0$ we have the case of one real and two complex roots. Three steady states exist thus when

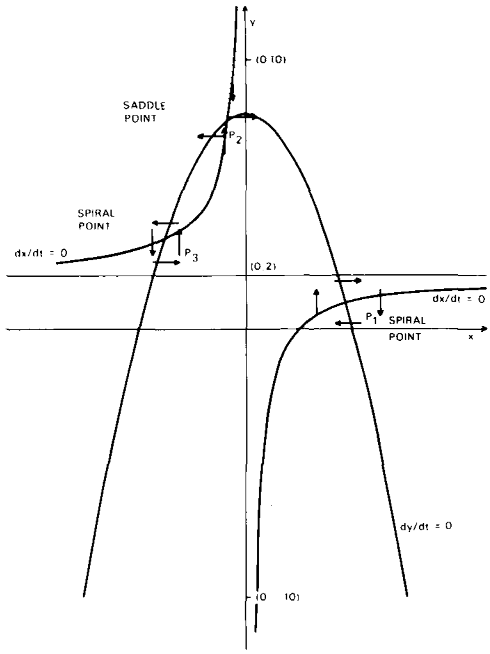

Fig. 1. Representation of the steady states P_1, P_2 and P_3. The parabola is the curve on which $dy/dt = 0$, while $dx/dt = 0$ on the hyperbola. The horizontal line through (0, 2) is an asymptote for the hyperbola. The intersections are the steady states. The arrows indicate the direction of the trajectory at points on the parabola or the hyperbola as deduced from the basic equations.

$$|x_E| < [\tfrac{2}{27}(y_E - 2)^3]^{1/2} \tag{2.7}$$

Equation (2.7) can be satisfied only if $y_E > 2$.

The values of the three real roots are

$$x_{sj} = 2\left[\frac{2(y_E - 2)}{3}\right]^{1/2} \cos\left(\tfrac{1}{3}\phi + j.\frac{2\pi}{3}\right), \tag{2.8}$$

$j = 0, 1, 2$

where ϕ is evaluated from the expression

$$\cos\phi = \frac{x_E}{\sqrt{\frac{2}{27}(y_E - 2)^3}} \tag{2.9}$$

Returning to Fig. 1 which corresponds to the case of three steady states we may investigate the trajectories in the immediate neighbourhood of the three intersections P_1, P_2 and P_3. Using the basic equations for the system and the facts that $dx/dt = 0$ on the hyperbola and $dy/dt = 0$ on the parabola we may deduce the direction of the trajectory in four points surrounding the steady state. In this way we find that P_1 and P_3 are so-called spiral points, while P_2 is a saddle point. The point P_2 is therefore an unstable steady state, while P_1 and P_3 may be stable or unstable depending on whether the spiral approaches the steady state or goes away from it. This question can be settled by a linear stability analysis.

We consider therefore an arbitrary steady state (x_s, y_s). Linearizing the basic equations we get

$$\frac{dx'}{dt} = \tfrac{1}{2}x_s y' + \tfrac{1}{2}y_s x' - x'$$
$$\frac{dy'}{dt} = -x_s x' - y' \tag{2.10}$$

where perturbation quantities are denoted by primes. We seek solutions of the form

$$(x', y') = (x_0, y_0)e^{\sigma t} \tag{2.11}$$

where σ is the eigenvalue. $\sigma_r > 0$ *indicates* instability. Using the usual procedure of substituting (2.11) in (2.10) and finding the conditions for non-trivial solutions by setting the determinant to zero we find that

$$\sigma = \tfrac{1}{4}[(y_s - 4) \pm (y_s^2 - 8x_s^2)^{1/2}] \tag{2.12}$$

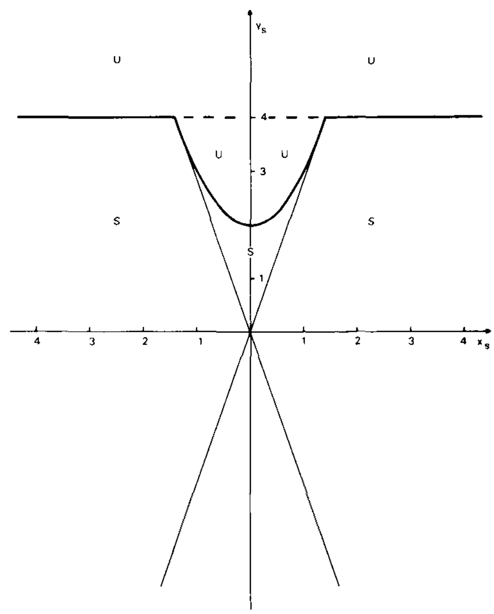

Fig. 2. The stability diagram in the (x_s, y_s) plane. The straight lines through the origin are $y_s = \pm 2\sqrt{2}x_s$.U and S indicate unstable and stable regions, respectively.

Considering first the region in which $y_s^2 < 8x_s^2$ we find that $\sigma_r > 0$ if $y_s > 4$. On the other hand, if $y_s^2 > 8x_s^2$, then σ is real. The eigenvalue σ will certainly be positive if $y_s > 4$. In addition, σ will be positive for $y_s < 4$ if

$$y_s^2 - 8x_s^2 > (4 - y_s)^2 \tag{2.13}$$

or

$$y_s > x_s^2 + 2 \tag{2.14}$$

Fig. 2 shows the stable and unstable regions in the (x_s, y_s) plane. It is naturally preferable to express the stability criteria

$$x_s^2 + 2 < y_s < 4 \text{ and } y_s > 4 \tag{2.15}$$

in terms of x_E and y_E and to derive a stability diagram in the (x_E, y_E) plane. Such an analysis is presented in appendix I, and the results are given in Fig. 3.

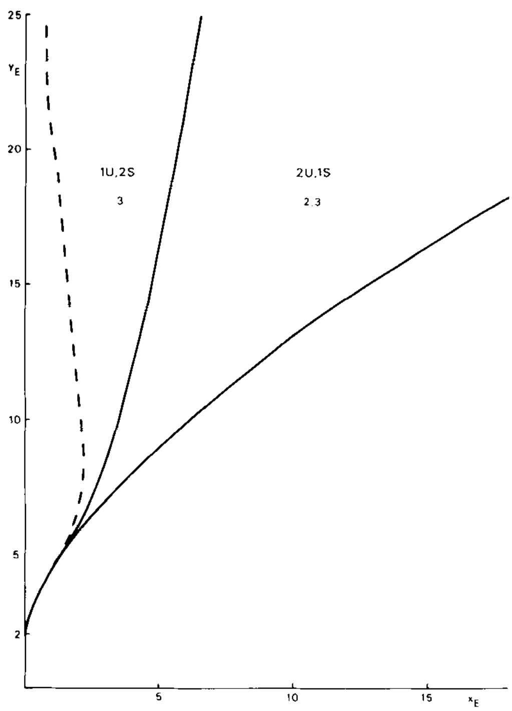

Fig. 3. The stability diagram in the (x_E, y_E) plane. The lower curve separates the region of one stable steady state below and three steady states above. The other full curve from $(\sqrt{2}, 5)$ upwards separates the region to the left of one unstable and two stable steady states and the region to the right of two unstable and one stable steady state. The dashed curve, determined by numerical experiments, separates the regions with and without "limit cycles" within the region of one unstable and two stable steady states.

Fig. 3 shows that in the region of three steady states there are two very different sub-regions. The region to the right-hand side, i.e. for large values of x_E and y_E, is characterized by two unstable and one stable steady state. It is to be expected and numerical experiments have confirmed that the single stable steady state is the asymptotic state, or, in other words, all trajectories wherever they start will eventually approach the stable steady state. The remaining part of the region is characterized by one unstable and two stable steady states. In this case we know only that if we start a trajectory close to the unstable steady state it will move away from the state, but the linear stability analysis cannot tell us which steady state will be the asymptotic state. For all the points in the region with one unstable and two stable steady states we carried out a numerical experiment. We selected 36 initial states on a small circle with the unstable steady state as centre. For each initial state we carried out a numerical integration until a steady state was reached. Based upon the results of these numerical experiments it is possible to sub-divide the region of one unstable and two stable steady states in two sub-regions sub-divided by the dashed line entered in Fig. 3.

The region to the right of the dashed line in Fig. 3 consists of points where all the trajectories surrounding the point P_2 in Fig. 1 will have the point P_1 as the asymptotic steady state.

The region to the left of the dashed line, on the other hand, are those points where some of the trajectories will have P_1 as the asymptotic state while others approach P_3 for large times.

To illustrate the behaviour in some of the cases mentioned above, we have prepared the following figures. Fig. 4 shows a case of two unstable and one stable steady state. The dashed lines in Fig. 4 show the parabola and the hyperbola used in Fig. 1. In this case both P_2 and P_3 are unstable steady states although P_2 is an unstable saddle point and P_3 is an unstable spiral point. A trajectory starting close to P_2 will either go to the right and approach P_1 in a spiral for large times or it will go to the left, go around P_3 and then approach P_1 in a spiral. On the other hand, a trajectory starting close to P_3 will spiral out, approach P_2, but since this state is unstable it will eventually deviate from P_2 and will finally approach P_1. All these trajectories are indicated in Fig. 4.

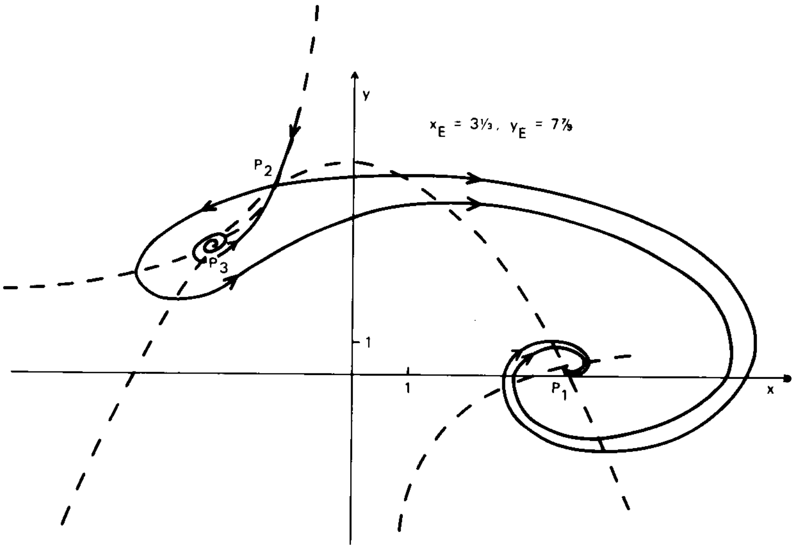

Fig. 4. Trajectories in the case: two unstable steady states (P_2 and P_3) and one stable steady state (P_1). The dashed curves are the parabola and the hyperbola from Fig. 1.

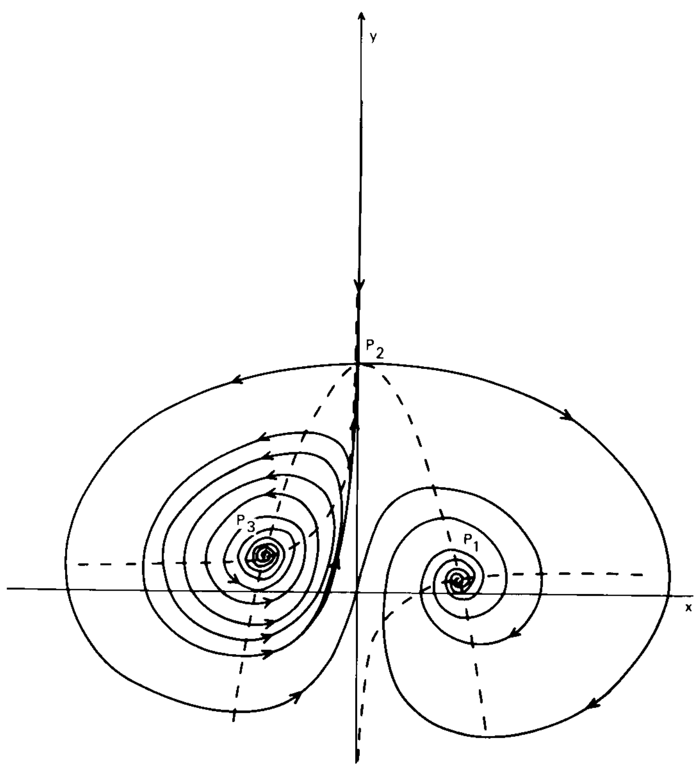

Fig. 5. Trajectories for the case $x_E = 3$, $y_E = 20$ with one unstable steady state P_2 and two stable steady states P_1 and P_3. The dashed curves are again the parabola and the hyperbola from Fig. 1. P_3 is a stable spiral point surrounded by an unstable limit cycle determined by a backward numerical integration.

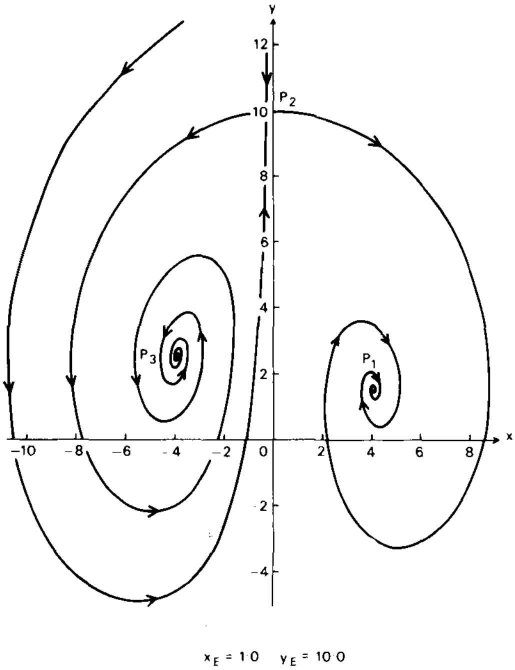

Fig. 6. Trajectories in the case of two stable steady states (P_1 and P_3) and one unstable (P_2) with $x_E = 1$ and $y_E = 10$.

Fig. 5 shows a case of one unstable and two stable steady states. The unstable steady state is as usual marked by P_2 and the two stable states as P_1 and P_3. It is seen that any trajectory starting close to P_2 will eventually approach P_1. The behaviour in the region surrounding P_3 can be explored by numerical integrations in which the time is reversed. An initial state close to P_3 is selected, and an integration of the basic non-linear equations with t replaced by $-t$ is carried out. It turns out that the "reversed" trajectory is a spiral which at large times approaches a curve, normally called an unstable "limit cycle". This means that any trajectory starting inside the "limit cycle" will approach P_3 for large positive times. On the other hand, a trajectory starting just outside the "limit cycle" will first depart from the limit curve, then approach P_2 and eventually come to P_1 as indicated in Fig. 5. The area in Fig. 3 inside which we have an unstable "limit cycle" around P_3 is limited by the dashed curve and the curve separating the regions with one unstable, two stable and two unstable, one stable steady states.

Fig. 6 also shows a case of one unstable and two stable steady states. This case is, however, in the region of the (x_E, y_E)-plane (Fig. 3) where no "limit cycle" exists. The trajectories separating the

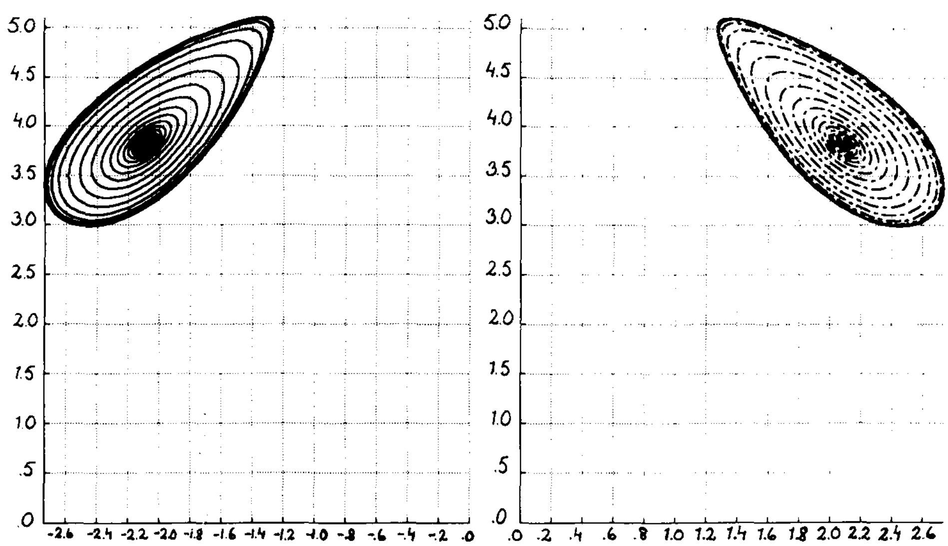

Fig. 7. "Limit cycles for $x_E = 1.9$, $y_E = 6.0$ with the initial condition $x_0 = -2.1$, $y_0 = 3.8$ and to the right for $x_E = -1.9$, $y_E = 6.0$, with the initial condition $x_0 = 2.1$, $y_0 = 3.8$.

regions containing all trajectories ending up in P_1 and P_3 respectively are called separatrices of the saddle point P_2. Separatrices directed towards the saddle point thus divide the (x, y)-plane into two regions, one containing all trajectories having P_1 as their limit point and the other containing all trajectories having P_3 as their limit point. These ingoing separatrices are unstable with respect to small perturbations around them. Therefore, to find them numerically we integrated eq. (2.3) backwards in time with initial values close to P_2.

We remarked earlier in connection with Fig. 3 that the stability diagram is symmetric around the y_E-axis. The non-linear trajectories are also symmetrical around the y-axis. An example is shown in Fig. 7 in which the left side shows a "limit cycle" calculated for $x_E = 1.9$ and $y_E = 6.0$ with the initial condition $x_0 = -2.1$, $y_0 = 3.8$ and t replaced by $-t$. The right-hand side of Fig. 7 shows the corresponding calculation for $x_E = -1.9$, $y_E = 6.0$, $x_0 = 2.1$, $y_0 = 3.8$. It is seen that there exists symmetry around the y-axis.

To summarize the results obtained in this section a "catastrophe surface" for the model has been

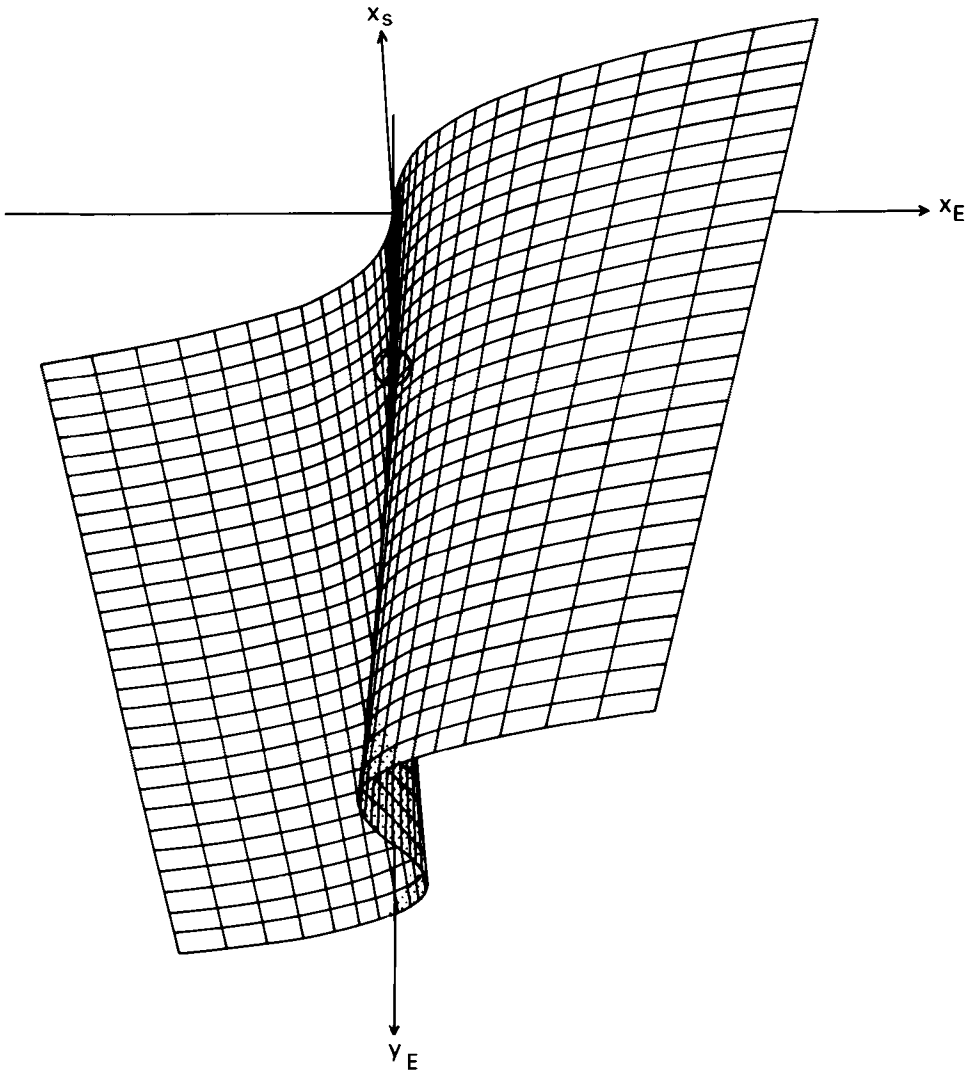

Fig. 8. Catastrophe surface for the two-dimensional model. The bifurcation point is denoted ⊙ and the dotted area corresponds to an unstable steady state.

constructed. Investigation of the number of steady states obtained for various values of x_E and y_E, can be seen as a bifurcation problem with respect to the two parameters x_E and y_E. Equation (2.5) gives the form of the "catastrophe surface", and rewriting it as

$$x_E = \frac{x_s^3}{4} - \frac{x_s}{2}(y_E - 2) \tag{2.16}$$

enables us to plot the surface. Fig. 8 shows this surface and it can be seen from the figure that we have a cusp catastrophe, the bifurcation point occurring at $x_E = 0$, $y_E = 2$. For x_E and y_E values inside the cusp (bounded by the folds on the surface) we have three values of x_s for each pair of x_E, y_E, outside the cusp only one x_s is possible. Going back to Fig. 3, the curve separating the regions of one and three steady states is a projection of the cusp on the x_E, y_E plane. The only difference is that Fig. 8 also involves negative x_E values.

Looking at the catastrophe surface in Fig. 8, we see the surface from above. The top pleat corresponds to the x_s value of P_1 for a given value of (x_E, y_E). The bottom pleat is P_3, while the middle pleat (inside the fold) gives the x_s of P_2. As P_2 always is unstable, the middle pleat represents an unstable steady-state while the top and bottom pleats are unstable near the fold and stable further away from it. The unstable part of the surface is dotted in Fig. 8.

3. Three component model

The model used in section 3 may naturally be applied with an arbitrary number of components. The two component model analysed in the previous section will in this section be replaced with a three component model. The purpose is to show the variety of solutions obtained even in this simple case.

The equations for the model are basically reproduced from Wiin-Nielsen (1976) but here forcing and dissipation are added. With the scaling used in this paper they become

$$\frac{dx}{dt} = \tfrac{1}{2}xy + \tfrac{1}{2}yz - \varepsilon x + x_E$$

$$\frac{dy}{dt} = -\tfrac{1}{2}x^2 + xz - \varepsilon y + y_E \tag{3.1}$$

$$\frac{dz}{dt} = \quad -\tfrac{3}{2}xy - \varepsilon z + z_E$$

where ε is a tracer in front of the dissipation terms, i.e. ε is either equal to zero or one.

Before investigating the steady states and their local stability, we turn to the global stability problem. We want to see what happens when $\sqrt{x^2 + y^2 + z^2} \to \infty$. Define the vectors $\mathbf{r} = (x, y, z)$ and $\mathbf{r}_E = (x_E, y_E, z_E)$.

Multiplying dx/dt by x, dy/dt by y and dz/dt by z in (3.1), summing and setting $\varepsilon = 1$ we obtain

$$\frac{d|\mathbf{r}|}{dt} = |\mathbf{r}_E| \cos \delta - |\mathbf{r}| \tag{3.2}$$

where δ is the angle between the vectors $\mathbf{r}$ and $\mathbf{r}_E$. For a given $|\mathbf{r}_E|$ eq. (3.2) states that it is always possible to make $d|\mathbf{r}|/dt$ less than zero by taking $|\mathbf{r}|$ sufficiently large. The system thus always tries to return towards the origin when displaced sufficiently far away from it. This does not mean that we always have a stable steady state. It only tells us that a time dependent solution of (3.1) can never "blow up".

Returning to the local stability problem, we linearize (3.1) around a steady state (x_s, y_s, z_s) obtaining

$$\frac{dx'}{dt} = (\tfrac{1}{2}y_s - \varepsilon)x' + \tfrac{1}{2}(x_s + z_s)y' + \tfrac{1}{2}y_s z'$$

$$\frac{dy'}{dt} = (z_s - x_s)x' \quad - \varepsilon y' + x_s z' \tag{3.3}$$

$$\frac{dz'}{dt} = \quad -\tfrac{3}{2}y_s x' \quad - \tfrac{3}{2}x_s y' - \varepsilon z'$$

where the primes indicate infinitesimal deviations from the steady state. We seek solutions to (3.3) of the form exp (σt), where σ is the complex eigenvalue. Substitution of this form of solution in (3.2) leads to a set of three homogeneous linear equations. They will have nontrivial solutions if their determinant is zero. This condition leads to the eigenvalue equation

$$(\sigma + \varepsilon)^3 - \tfrac{1}{2}y_s(\sigma + \varepsilon)^2 + \tfrac{3}{4}y_s^2 + 2x_s^2 - \tfrac{1}{2}z_s^2(\sigma + \varepsilon) + \tfrac{3}{4}x_s y_s(2z_s - x_s) = 0 \tag{3.4}$$

3.1. *Conservative case*

Considering first a conservative system without forcing the dissipation we set $\varepsilon = 0$ and $x_E = y_E = z_E = 0$ in (3.1), obtaining

$$\begin{aligned}\frac{dx}{dt} &= \tfrac{1}{2}xy + \tfrac{1}{2}yz \text{ (a)}\\ \frac{dy}{dt} &= -\tfrac{1}{2}x^2 + xz \text{ (b)}\\ \frac{dz}{dt} &= -\tfrac{3}{2}xy \text{ (c)}\end{aligned} \tag{3.5}$$

It is seen from the last equation in (3.5) that a steady state must have either $x = 0, y \neq 0$; $x \neq 0, y = 0$; or $x = 0, y = 0$. In the first case we note that (b) and (c) of (3.5) are satisfied and that (a) requires $z = 0$.

A steady state is therefore $(0, y_s, 0)$. In the second case we satisfy (a) and (c), while (b) leads to $x_s = 2z_s$. Another steady state is therefore $(2z_s, 0, z_s)$. In the third case we find that all equations in (3.5) are satisfied for an arbitrary value of z_s. The final steady state is $(0, 0, z_s)$. From (3.5) we can furthermore derive the result that $x^2 + y^2 + z^2$ is a conservative quantity for the system (3.5), i.e. the kinetic energy is constant along the trajectory. Without loss of generality we shall in the following select an initial state for which $x_0^2 + y_0^2 + z^2{}_0 = 1$. In this case we find that the steady states are

$$(0, \pm 1, 0),\ \left(\pm\frac{2}{\sqrt{5}}, 0, \pm\frac{1}{\sqrt{5}}\right),\ (0, 0, \pm 1)$$

Applying the eigenvalue equation (3.4) with $\varepsilon = 0$ we get the following stability results for these steady states:

$$\begin{aligned}
&(0, 1, 0) &&: \sigma_1 = 0, \quad \sigma_{2,3} = \frac{1}{4} \pm \frac{1}{4} i \sqrt{11}\\
&(0, -1, 0) &&: \sigma_1 = 0, \quad \sigma_{2,3} = -\frac{1}{4} \pm \frac{1}{4} i \sqrt{11}\\
&\left(\frac{2}{\sqrt{5}}, 0, \frac{1}{\sqrt{5}}\right) &&: \sigma_1 = 0, \quad \sigma_{2,3} = \pm i \sqrt{\frac{3}{2}}\\
&\left(-\frac{2}{\sqrt{5}}, 0, -\frac{1}{\sqrt{5}}\right) &&: \sigma_1 = 0, \quad \sigma_{2,3} = \pm i \sqrt{\frac{3}{2}}\\
&(0, 0, 1) &&: \sigma_1 = 0, \quad \sigma_{2,3} = \pm \frac{1}{\sqrt{2}}\\
&(0, 0, -1) &&: \sigma_1 = 0, \quad \sigma_{2,3} = \pm \frac{1}{\sqrt{2}}
\end{aligned}$$

From these results we observe that the only stable steady state is $(0, -1, 0)$. The steady states $(0, 1, 0)$, $(0, 0, 1)$ and $(0, 0, -1)$ are unstable, while the states $(2/\sqrt{5}, 0, 1/\sqrt{5})$ and $(-2/\sqrt{5}, 0, -1/\sqrt{5})$ are neutral. The non-zero imaginary part in the states $(0, 1, 0)$ and $(0, -1, 0)$ indicates that the first state is an unstable spiral point while the second is a stable spiral point. The two neutral states are characterized by closed trajectories in the linear case because the real part is zero. The two unstable states $(0, 0, 1)$ and $(0, 0, -1)$ are saddle points. These types apply naturally to the solutions of the linearized equations (3.3), and they are therefore only applicable in the immediate vicinity of the steady state.

The nature of the solutions to the non-linear equations (3.5) is found by numerical integrations of these equations. The general behaviour of the solutions is shown in Fig. 9. The trajectories shown in this figure are on the unit sphere. The spiral point in the lower right hand side of the figure is the unstable state $(0, 1, 0)$. Trajectories starting close to this point will eventually end up in the stable spiral point $(0, -1, 0)$ as indicated by the dashed curve (on the backside of the sphere). The saddle point $(0, 0, 1)$ is also seen on the figure. The separatrices have been constructed by numerical procedures. Note, in particular, the region to the lower left of the point $(0, 0, 1)$. Within this region all trajectories are closed curves on the sphere around the neutral point $(2/\sqrt{5}, 0, 1/\sqrt{5})$. The region is limited by the closed curve which is made up by a pair of separatrices to the saddle point $(0, 0, 1)$. A corresponding region surrounds the neutral point $(-2/\sqrt{5}, 0, -1/\sqrt{5})$, but this point is not indicated on the figure. It is thus seen that the surface of the sphere can be divided in three regions: one region surrounds the neutral point $(2/\sqrt{5}, 0, 1/\sqrt{5})$ and this region comes infinitesimally close to $(0, 0, 1)$. All trajectories inside the region are closed curves on the surface of the sphere. The second region is analogous to the first, but surrounds the neutral point $(-2/\sqrt{5}, 0, -1/\sqrt{5})$. This region comes infinitesimally close to the unstable saddle point $(0, 0, -1)$. The third region is the remaining part of the unit sphere. All trajectories in this region will eventually end in the stable point $(0, -1, 0)$.

We have thus seen that the solutions to the three component system without forcing and dissipation are either periodic solutions of an oscillatory nature

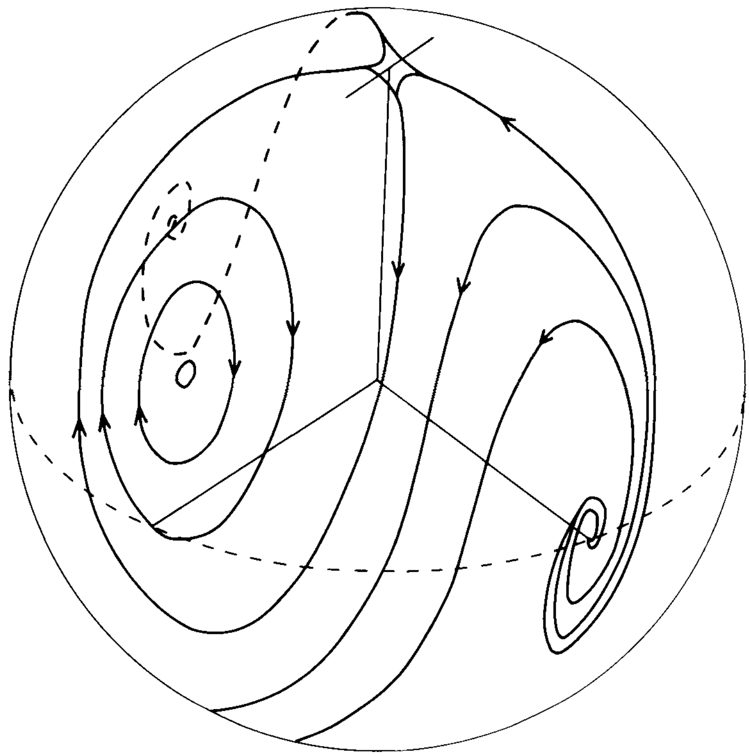

Fig. 9. Trajectories of a three component system without forcing and dissipation. All trajectories are on the surface of the unit sphere. The unstable spiral point in the lower right part of the figure is (0, 1, 0), while the stable spiral point (dashed curve) on the back of the sphere is (0, −1, 0). The neutral point surrounded by trajectories in the left side of the figure is $(2/\sqrt{5}, 0, 1/\sqrt{5})$, while the saddle point at the top of the figure is (0, 0, 1).

in the two regions surrounding the neutral points or non-periodic solutions which have the same asymptotic state (0, −1, 0). The type of solution is determined entirely by the initial conditions.

3.2. *Forced and dissipative case*

We consider next the system with forcing and dissipation ($\varepsilon = 1$). First we take $x_E \neq 0$, but keep $y_E = z_E = 0$ (forcing only on the large scale component). This changes the behaviour of the system drastically when compared to the conservative case. It can be shown that the system has one steady state only, and a numerical investigation of the eigenvalue equation (3.4) indicates that this single steady state is always stable.

Keeping $\varepsilon = 1$ but taking $y_E \neq 0$, and $x_E = z_E = 0$ we have forcing only on the middle scale component. In this case there is also only one steady state with $x_s = 0$, $y_s = y_E$ and $z_s = 0$. The stability of this steady state is given by eq. (3.4), and the eigenvalues are

$$\sigma_1 = -1,\ \sigma_{2,3} = \tfrac{1}{4}(y_E - 4) \pm i\tfrac{1}{4}y_E\sqrt{11}$$

For $y_E < 4$ the steady state is thus stable, but for $y_E > 4$ the system is locally unstable as the real part of $\sigma_{2,3} > 0$. Going back to the discussion of the global stability, this local instability around the single steady state indicates that we have a limiting trajectory around the steady state. Numerical experiments show that this is the case. An example is shown in Fig. 10 for $y_E = 5$.

In the case where $z_E \neq 0$, $x_E = y_E = 0$ and $\varepsilon = 1$, we have a slightly more complicated situation. The steady state(s) (x_s, y_s, z_s) must satisfy

$$\begin{aligned} &\tfrac{1}{2}x_s y_s + \tfrac{1}{2}y_s z_s - x_s = 0 \text{ (a)} \\ &-\tfrac{1}{2}x_s^2 + x_s z_s - y_s = 0 \text{ (b)} \\ &-\tfrac{3}{2}x_s y_s - z_s + z_E = 0 \text{ (c)} \end{aligned} \qquad (3.6)$$

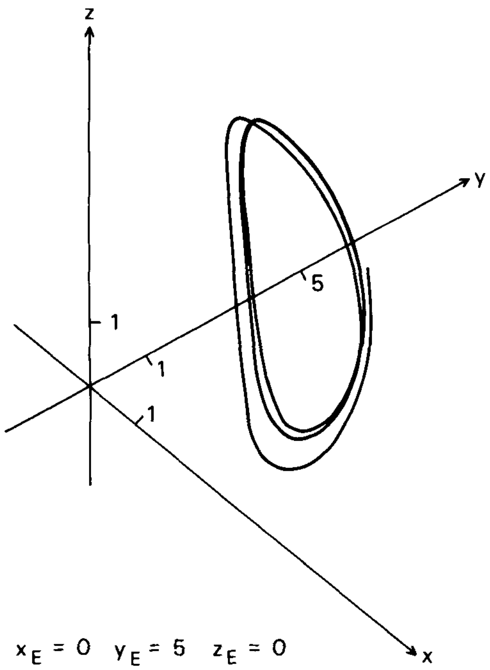

Fig. 10. Three-dimensional perspective view of the stable limit behaviour obtained in the three component cases for $x_E = 0, y_E = 5$ and $z_E = 0$.

Eliminating z_s from eq. (3.6) we get the following equations in y_s and x_s

$$x_s^2 = \frac{2}{3}\frac{y_s^2}{\frac{4}{3} - y_s} \quad \text{(a)}$$

$$x_s = \frac{2}{3}\frac{z_E y_s}{y_s^2 - \frac{2}{3}y_s + \frac{4}{3}} \quad \text{(b)} \tag{3.7}$$

From (3.7a) it follows that $y_s < \frac{4}{3}$, and combining (3.7a) and (3.7b) we obtain

$$z_E^2 y_s^2 (\tfrac{4}{3} - y_s) = \tfrac{3}{2} y_s^2 (y_s^2 - \tfrac{2}{3} y_s + \tfrac{4}{3})^2 \tag{3.8}$$

One steady state is thus always $y_s = 0$ (implying $x_s = 0$ and $z_s = z_E$), but for some values of z_E additional steady states are obtained. Rewriting (3.8) as

$$z_E = \sqrt{\frac{3}{2}}\frac{(y_s^2 - \frac{2}{3}y_s + \frac{4}{3})}{\sqrt{\frac{4}{3} - y_s}}, \qquad y_s < \tfrac{4}{3} \tag{3.9}$$

we can investigate this graphically. Differentiating (3.9) with respect to y_s, we find that $z_E(y_s)$ only has one extremum, for $y_s = 1 - \sqrt{\frac{23}{27}}$. In Fig. 11 a plot of $z_E(y_s)$ is shown. For z_E-values larger than $z_E(1 - \sqrt{\frac{23}{27}}) = z_{E,\text{crit}} = 1.4073$ we thus have a total of three steady states, one with $y_s = 0$ and the two others given by the intersection of a line z_E = constant with the curve in Fig. 11.

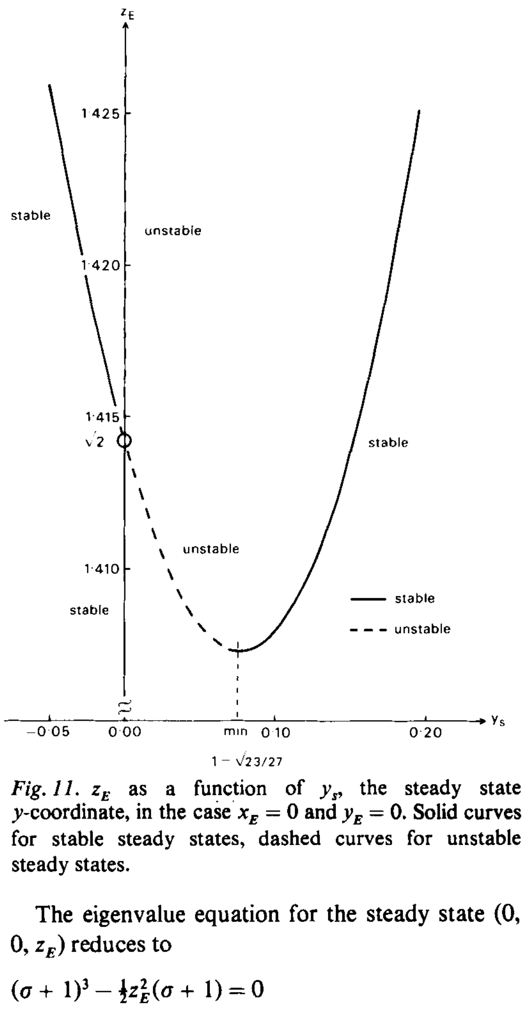

Fig. 11. z_E as a function of y_s, the steady state y-coordinate, in the case $x_E = 0$ and $y_E = 0$. Solid curves for stable steady states, dashed curves for unstable steady states.

The eigenvalue equation for the steady state (0, 0, z_E) reduces to

$$(\sigma + 1)^3 - \tfrac{1}{2} z_E^2 (\sigma + 1) = 0$$

giving

$$\sigma_1 = -1, \sigma_{2,3} = -1 \pm \frac{z_E}{\sqrt{2}}$$

This steady state is always stable for $z_E < \sqrt{2}$, and unstable for $z_E > \sqrt{2}$. Numerical investigations for the other steady states show the stability properties indicated along the curve in Fig. 11. We note from Fig. 11 that for $z_E > z_{E,\text{crit}}$ we obtain three steady states. The stability properties are always such that an unstable steady state is surrounded by two stable ones even though the stability properties of (0, 0, z_E) shift when $z_E = \sqrt{2}$ ($>z_{E,\mathrm{crit}}$). The unstable steady state always has purely real eigenvalues, while the two stable ones may have imaginary parts. A numerical integration with $z_E = 3$ is shown in Fig. 12. The initial values were chosen close to the unstable steady state, and integrations both backwards and forward in time were performed. For integrations forward in time the trajectories end up in one of the stable steady states. The asymptotic steady state depends on the initial value.

Through the unstable steady state there must be a surface separating two regions, one region containing all trajectories ending up in one of the stable steady states and the other region containing all trajectories ending up in the other stable steady state. All trajectories on the surface score a direct hit on the unstable steady state, and the surface is thus a three-dimensional analogy to the separatrices discussed in section 2.

In Fig. 12 the trajectory coming from the right hand side of the figure where y is large and positive, approaches the unstable steady-state P_2 and having passed close to P_2 it asymptotes towards P_3. This trajectory has been found numerically by choosing an initial state close to P_2 and integrating both backward and forward in time. The part of the trajectory spiralling around the y-axis is thus very close to the separating surface discussed earlier, and it suggests that the separating surface is pear shaped with the bottom of the pear at (0, 0, z_E) and the symmetry axis of the pear along the y-axis. It seems likely that the region containing all trajectories having P_3 as their asymptotic steady state comes asymptotically close to the y-axis as y goes to infinity, and in appendix II an analytical argument for this is presented.

Finally we have also briefly considered the case when there is forcing both y_E and z_E but $x_E = 0$. Dissipation is also included. The steady states (x_s, y_s, z_s) of this system are given by

$$\begin{aligned} &\tfrac{1}{2}x_s y_s + \tfrac{1}{2}y_s z_s - x_s = 0 \text{ (a)} \\ &-\tfrac{1}{2}x_s^2 + x_s z_s - y_s + y_E = 0 \text{ (b)} \\ &-\tfrac{3}{2}x_s y_s - z_s + z_E = 0 \text{ (c)} \end{aligned} \tag{3.10}$$

Eliminating x_s and z_s between these equations, we obtain a single equation in y_s. Writing this equation as $y_E(y_s, z_E)$, we can plot a "catastrophe" surface,

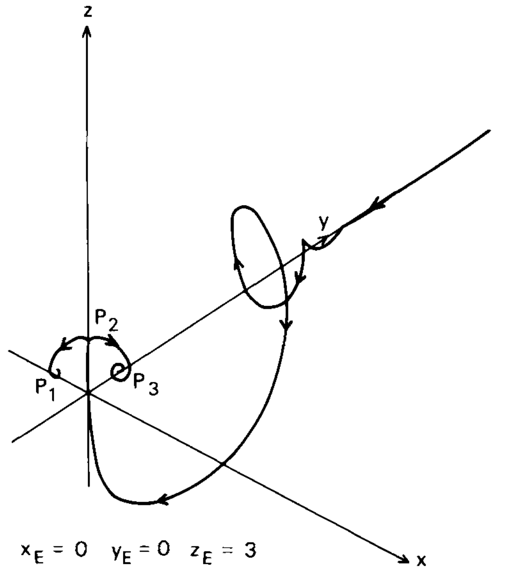

Fig. 12. Three dimensional perspective view of trajectories when $x_E = 0$, $y_E = 0$ and $z_E = 3$. P_1 and P_3 are stable steady states while Px_2 is unstable.

just as was done for the two-component system in section 3. The equation for the surface is

$$y_E = y_s \left[1 + \tfrac{2}{3}z_E^2 \frac{(y_s - \frac{4}{3})}{(y_s^2 - \frac{2}{3}y_s + \frac{4}{3})^2}\right] \tag{3.11}$$

and a plot of the surface is given in Fig. 13. As (3.11) is a quintic equation in y_s a maximum of five steady states for given values of (y_E, z_E) is expected. Fig. 14 shows cross-sections of the surface for some different values of z_E. We see from the figures that for sufficiently large z_E values we have one fold in the surface giving rise to a cusp catastrophe. For even larger z_E values a second fold occurs giving rise to a second cusp catastrophe. In Fig. 14 an example of five steady states is shown for $y_E = 7.5$ and $z_E = 10.0$. The line $y_E = 7.5$ intersects the curve for $z_E = 10.0$ five times.

Figs. 13 and 14 indicate the existence of up to five steady states for a certain parameter range. A detailed investigation of the stability properties of all these steady states is possible, but it is not expected that such an analysis would add significantly to the types of behaviour discussed earlier.

4. Conclusions

The purpose of this paper was to study the behaviour of solutions to an equation containing the advective non-linearity, and the restrictions

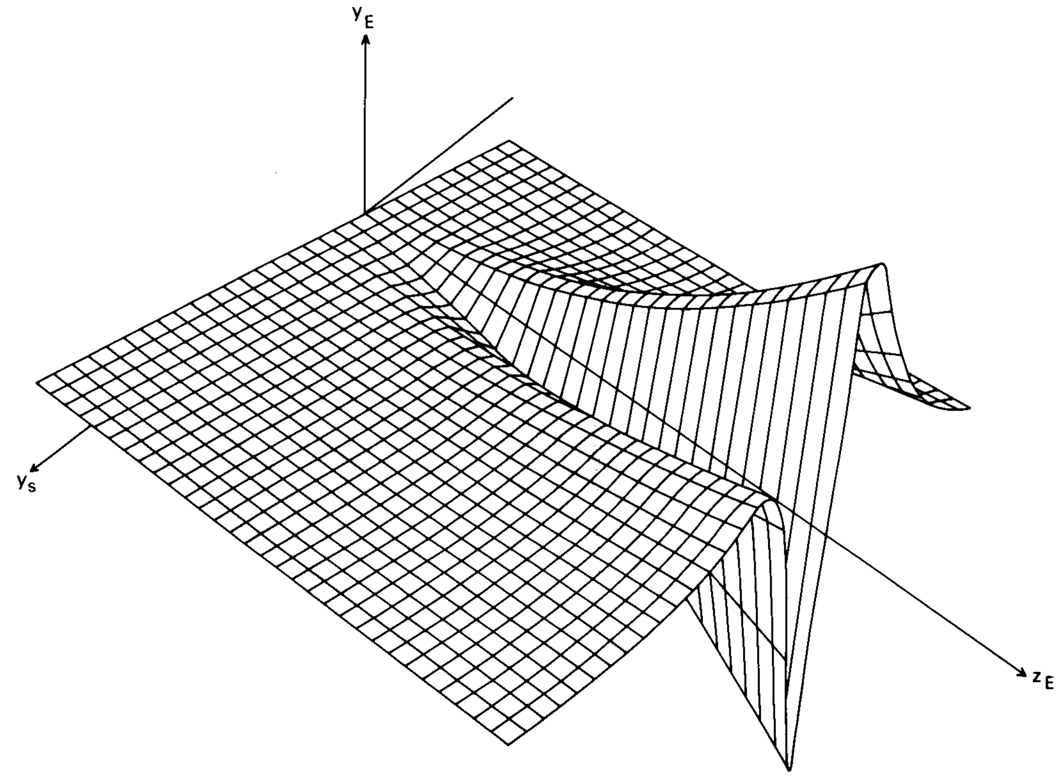

Fig. 13. Catastrophe surface for the three component case with forcing in the y- and z-component.

imposed upon the solutions by the interplay between forcing, dissipation and the non-linearity.

The behaviour of the atmosphere on medium and large time scales is of a non-linear nature. It is likely that the atmosphere for a given forcing and dissipation has a multitude of steady states. The determination of these states is a difficult problem, and it is significant that all general circulation models result in a climatic state which resembles the present climate. In an attempt to illustrate this problem by particularly simple examples we have analysed the behaviour of some extremely simple non-linear systems restricted to a few spectral components. For these systems it is relatively straightforward to determine the steady states and to explore the linear stability of these states. The non-linear behaviour of the systems can be determined by numerical experimentation. Sections 2 and 3 describe the main result of such an analysis. It can be argued that qualitatively we obtain the same results in the two- and three-component cases. Forcing on the largest scale only results in only one stable steady state, while forcing on the smaller scale components gives rise to cusp catastrophes and "limit cycle" behaviour.

Comparing our analysis with the one by Vickroy and Dutton (1979), (hereafter denoted V&D), one find a striking similarity between our two-component system and their three-component one. They have the same type of bifurcation surface as the one given in Fig. 8, the main difference lies in the stability of the limit cycle. V&D obtain a stable limit cycle whereas ours is unstable. Even though V&D have three components in their system, it does not contain more than two scales of motion. Three equations are still needed in order to obtain non-trivial non-linear interactions (Lorenz, 1960). Our three component system may thus correspond to a quasi-geostrophic low order system involving three scales of motion.

A distinct feature of the systems studied here is the relatively regular behaviour of the phase space orbits. We have not found any strange attractors as described by Lorenz (1963) in connection with an investigation of a low order convective system. Lorenz argued that if the non-periodicity displayed

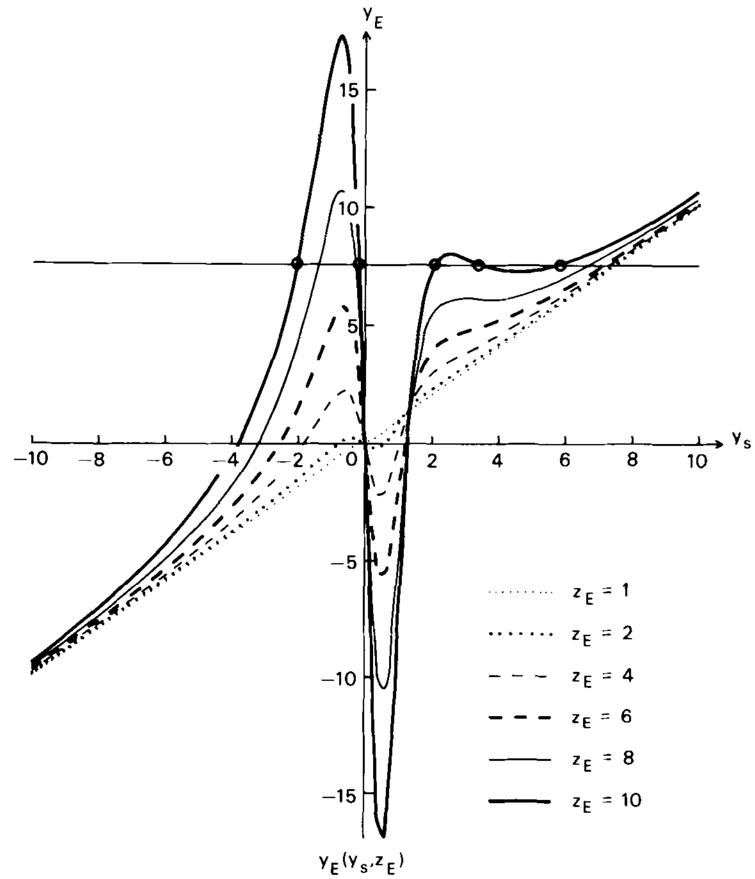

Fig. 14. Cross sections with z_E = constant of the surface given in Fig. 13. The straight line $y_E = 7.5$ is drawn to give an example of the number of intersections with the cross section curve $z_E = 10$, thus giving the number of steady states.

by his low order system could be carried over to the atmosphere it would imply that unless the initial state is known exactly the atmosphere would be essentially unpredictable. Our results indicate that it is only within certain subsets of phase space that the initial conditon has to be known exactly in order for the trajectory to arrive at the correct asymptotic state. Other subsets of phase space can be seen as "attractor basins" of one of the stable steady states. Within these "attractor basins" an uncertainty in the initial state will not affect the asymptotic state. If, however, the forcing also varies in time it may be that a trajectory in the "attractor basin" of one stable steady state may suddenly find itself in the "attractor basin" of another stable steady state. Within certain regions of the forcing phase space it is thus also important to know the forcing exactly while uncertainties in other regions do not have such a drastic effect on the asymptotic states.

It is unfortunately not possible to use the same procedures as the ones used here for multi-component systems because the determination of all the steady states becomes impossible. The results of the analysis of simple low-order systems should therefore be considered as indicating certain mechanisms which may or may not be present in systems with many components. The behaviour of the low-order systems indicates that multiple steady states may exist, that two or more steady states may be stable, and that the total behaviour of the system is determined by the nature of the forcing. It is thus believed that the analysis of the simple low-order systems is worthwhile because such an analysis may guide more general studies of systems with a large number of degrees of freedom.

5. Acknowledgements

The authors would like to thank Ulf Hansson and Åke Johansson at the Department of Meteorology, University of Stockholm and Aleksander Konstantinovic, ECMWF for programming help.

6. Appendix I

Transformation from the (x_s, y_s) to the (x_E, y_E) plane for the two-component case

We consider first the region

$$x_s^2 + 2 < y_s < 4 \tag{AI.1}$$

Since $y_E = y_s + \frac{1}{2}x_s^2$ we find that $2 < y_E < 5$ and furthermore that

$$x_s^2 < \tfrac{2}{3}(y_E - 2) \tag{AI.2}$$

Using the expression (2.8) for x_s we find that (AI.2) is equivalent to

$$-\tfrac{1}{2} < \cos\left(\tfrac{1}{3}\phi + j\frac{2\pi}{3}\right) < \tfrac{1}{2} \tag{AI.3}$$

Since $x_E > 0$ it follows that $0 < \phi < \frac{1}{2}\pi$ and thus $0 < \frac{1}{3}\phi < \frac{1}{6}\pi$. It is thus easy to see that the roots corresponding to $j = 0$ and $j = 1$ do not satisfy (AI.3) and consequently are stable steady states while the root corresponding to $j = 2$ does satisfy (AI.3) and therefore is the only unstable steady state. From

$0 < \cos\phi < 1$

we find that

$$x_E < [\tfrac{2}{27}(y_E - 2)^3]^{1/2}, \qquad 2 < y_E < 5 \tag{AI.4}$$

as a region with one unstable and two stable steady states.

We consider next the region

$$y_s > 4 \tag{AI.5}$$

leading to

$$x_s^2 < 2(y_E - 4); \qquad y_E > 4 \tag{AI.6}$$

Using again (2.8) for x_s we find from (AI.6) that it leads to the inequalities

$$-\left[\frac{3}{4}\frac{y_E - 4}{y_E - 2}\right]^{1/2} < \cos\left(\tfrac{1}{3}\phi + j\frac{2\pi}{3}\right) < \left[\frac{3}{4}\frac{y_E - 4}{y_E - 2}\right]^{1/2} \tag{AI.7}$$

It is convenient to define the angle θ by

$$\cos\theta = \left[\frac{3}{4}\frac{y_E - 4}{y_E - 2}\right]^{1/2}; \qquad 0 < \theta < \frac{\pi}{2} \tag{AI.8}$$

and we get from (AI.7) that it will be satisfied if

$$\theta < \tfrac{1}{3}\phi + j\frac{2\pi}{3} < \pi - \theta \tag{AI.9}$$

or

$$\pi + \theta < \tfrac{1}{3}\phi + j\frac{2\pi}{3} < 2\pi - \theta \tag{AI.10}$$

The object is now to investigate if the three roots satisfy either (AI.9) or (AI.10). We start by noting from (AI.8) that the right-hand side will vary monotonically between 0 for $y_E = 4$ and $\frac{1}{2}\sqrt{3}$ for y_E approaching infinity. It follows that

$$\tfrac{1}{6}\pi < \theta < \tfrac{1}{2}\pi \tag{AI.11}$$

Considering first the case $j = 0$ we have

$$0 < \tfrac{1}{3}\theta < \tfrac{1}{6}\pi < \theta \tag{AI.12}$$

showing that the first steady state is stable. For $j = 1$ we find

$$\tfrac{2}{3}\pi < \tfrac{1}{3}\phi + \frac{2\pi}{3} < \frac{5\pi}{6} \tag{AI.13}$$

If $\frac{1}{3}\phi + 2\pi/3$ shall be in the interval $[\theta, \pi - \theta]$ we must require that

$$\tfrac{1}{3}\phi + \tfrac{2}{3}\pi < \pi - \theta$$

or

$$\phi < \pi - 3\theta \tag{AI.14}$$

Since ϕ is positive it is seen that (AI.14) cannot be satisfied if

$$\pi - 3\theta < 0 \tag{AI.15}$$

leading to

$$\cos\theta < \tfrac{1}{2} \tag{AI.16}$$

and therefore

$$y_E < 5 \tag{AI.17}$$

The second steady state is therefore stable for $y_E < 5$. For $y_E > 5$ we find that (AI.14) will be satisfied if

$$x_E > -[\tfrac{2}{27}(y_E - 2)^3]^{1/2}\cos\left(3\arccos\left[\frac{3}{4}\frac{y_E - 4}{y_E - 2}\right]^{1/2}\right) \tag{AI.18}$$

The second steady state is therefore unstable if $y_E > 5$ and (3.32) is satisfied.

For $xj = 2$ we have

$$\tfrac{4}{3}\pi < \tfrac{1}{3}\theta + \frac{4\pi}{3} < \tfrac{3}{2}\pi \tag{AI.19}$$

If $\frac{1}{3}\theta + \frac{4}{3}\pi$ shall be in the interval $[\pi + \theta, 2\pi - \theta]$ we must require

$$\pi + \theta < \tfrac{1}{3}\phi + \tfrac{4}{3}\pi$$

or

$$\theta > 3\theta - \pi \tag{AI.20}$$

Equation (AI. 20) is always satisfied if $3\theta - \pi < 0$ leading to

$$y_E > 5 \tag{AI.21}$$

The third steady state is thus unstable if $y_E > 5$. For $y_E < 5$ we must require that (AI.20) is satisfied leading to

$$x_E < -[\tfrac{2}{27}(y_E - 2)^3]^{1/2} \cos\left(3 \arccos \left[\frac{3}{4}\frac{y_E - 4}{y_E - 2}\right]^{1/2}\right) \tag{AI.22}$$

The results of these analyses are summarized in Fig. 3 showing the regions in which the second and third steady states are unstable.

In the calculations above we have considered the case of three steady states. We shall finally consider the case when only one steady state exists. As shown below this state is always stable. The region of our steady state in the (x_E, y_E) plane is given by

$$x_E^2 > \tfrac{2}{27}(y_E - 2)^3 \tag{AI.23}$$

Since

$$\begin{aligned} y_E &= y_s + \tfrac{1}{2}x_s^2 \\ x_E &= -\tfrac{1}{2}x_s(y_s - 2) \end{aligned} \tag{AI.24}$$

we find after some calculations that (AI.23) in the (x_s, y_s) plane can be written in the form

$$(y_s - 2 - x_s^2)^2\,(8(y_s - 2) + x_s^2) < 0 \tag{AI.25}$$

(AI.23) corresponds therefore in the (x_s, y_s) plane to the region

$$y_s < 2 - \tfrac{1}{8}x_s^2 \tag{AI.26}$$

which is entirely in the stable region of Fig. 2.

The stability analysis in this section may be repeated for $x_E < 0$. The result is a stability diagram symmetrical to the diagram in Fig. 3 around the y_E axis.

7. Appendix II

Asymptotic properties for the three component system when $y \to \infty$

We will here examine the asymptotic properties of the three-component system with forcing only on the smallest scale, i.e. $z_E \neq 0$ and $x_E = y_E = 0$. To explain analytically the numerically obtained result that the y-axis is a stable limiting trajectory backwards in time (see Fig. 12) we note the following:

Replacing t by $-t'$ ($t' > 0$, backwards in time) in (3.1) with $x_E = y_E = 0$ and $\varepsilon = 1$ we get

$$\begin{aligned} \frac{dx}{dt'} &= -\tfrac{1}{2}xy - \tfrac{1}{2}yz + x \quad \text{(a)} \\ \frac{dy}{dt'} &= \tfrac{1}{2}x^2 - xz + y \quad \text{(b)} \\ \frac{dz}{dt'} &= \tfrac{3}{2}xy + z - z_E \quad \text{(c)} \end{aligned} \tag{AII.1}$$

Considering the motion only in a plane perpendicular to the y-axis, we combine (AII.1a) and (AII.1c) regarding y as a parameter. Linearizing these two equations around a point (x_0, z_0) we obtain

$$\begin{aligned} \frac{dx'}{dt'} &= \left(1 - \frac{y}{2}\right)x' - \frac{y}{2}z' \\ \frac{dz'}{dt'} &= \tfrac{3}{2}yx' + z' \end{aligned} \tag{AII.2}$$

The stability properties of this system of equations depend only on y, and it is found that they are stable for $y > 4$. The quasi steady state (x_0, z_0) of eqs. (AII.1a) and (AII.1c) is given by

$$\begin{aligned} x_0 &= z_E \frac{y}{\tfrac{3}{2}y^2 - y + 2} \quad \text{(a)} \\ z_0 &= z_E \frac{(2 - y)}{\tfrac{3}{2}y_2 - y + 2} \quad \text{(b)} \end{aligned} \tag{AII.3}$$

Both right-hand sides tend to zero as y approaches infinity, so this confirms that the y-axis is a stable quasi steady state for the motion in an (x, z) plane when y goes to infinity. What remains to be shown is that $dy/dt' > 0$ for x_0 and z_0 given by (AII.3). Inserting $x = x_0$ and $z = z_0$ in (AII.1b) one obtains

$$\frac{dy}{dt'} = \frac{2}{3}\frac{z_E^2\, y(y - \frac{4}{3})}{(y^2 - \frac{2}{3}y + \frac{4}{3})^2} + y \tag{AII.4}$$

The right-hand side of (AII.4) is always greater than zero for $y > \frac{4}{3}$. We have thus shown that all trajectories backwards in time of eqs. (3.6), having an initial state with $y > 4$, will asymptotically approach the y-axis.

REFERENCES

Charney, J. G. and DeVore, J. G. 1979. Multiple flow equilibria in the atmosphere and blocking. *J. Atmos. Sci. 36*, 1205–1216.

Chen, T. C. and Wiin-Nielsen, A. 1978. On nonlinear cascades of atmospheric energy and enstrophy in a two-dimensional spectral index. *Tellus 30*, 313–322.

Epstein, E. S. 1969. Stochastic-dynamic predictions. *Tellus 21*, 739–759.

Fjørtoft, R. 1953. On the changes in the spectral distribution of kinetic energy for two-dimensional nondivergent flow. *Tellus 5*, 225–230.

Fleming, R. J. 1971a. On stochastic-dynamic predictions, I The energetics of uncertainty and the question of closure. *Mo. Wea. Rev. 99*, 851–872.

Fleming, R. J. 1971b. On stochastic-dynamic predictions, II Predictability and utility, *Mo. Wea. Rev. 99*, 927–938.

Lorenz, E. N. 1960. Maximum simplification of the dynamic equations. *Tellus 12*, 243–254.

Lorenz, E. N. 1962. Simplified dynamic equations applied to the rotating-basin experiments. *J. Atmos. Sci. 19*, 39–51.

Lorenz, E. N. 1963. Deterministic nonperiodic flow. *J. Atmos. Sci. 20*, 130–141.

Pitcher, E. J. 1974. Stochastic dynamic predictions using atmospheric data. Ph.D. dissertation, University of Michigan (available through Library of Congress).

Platzman, G. W. 1964. An exact integral of complete spectral equations for unsteady one-dimensional flow. *Tellus 16*, 422–431.

Saltzman, B. 1970. Large-scale atmospheric energetics in the wave number domain. *Rev. Geophys. Space Phys. 8*, 289–302.

Steinberg, H. L., Winn-Nielsen, A. and Yang, C. H. 1971. On non-linear cascades in large-scale atmospheric flow. *J. Geophys. Res. 76*, 8829–8840.

Vickroy, V. G. and Dutton, J. A. 1979. Bifurcation and catastrophe in a simple, forced, dissipative quasi-geostrophic flow. *J. Atmos. Sci. 36*, 42–52.

Wiin-Nielsen, A. 1976. Predictability and climate variation illustrated by a low-order system. Proceedings of Seminar on Scientific Foundation of Medium-Range Weather Forecasts, ECMWF, 258–306.

Wiin-Nielsen, A. 1979a. Steady states and stability properties of a low-order barotropic system with forcing and dissipation. *Tellus 31*, 375–386.

Wiin-Nielsen, A. 1979b. On the asymptotic behaviour of a simple stochastic-dynamic system. *Geoph. and Astroph. Fluid Dynamics 12*, 295–311.

Yang, C. H. 1967. Nonlinear aspects of the large-scale motion in the atmosphere. Ph.D. dissertation, University of Michigan, 173 pp.

НЕЛИНЕЙНЫЕ ВЗАИМОДЕЙСТВИЯ НИЗКОГО ПОРЯДКА

Представлено исследование уравнения адвекции с ньютоновскими притоками тепла и диссипацией. В спектральном разложении простого уравнения адвекции сохраняются лишь несколько компонент, вращение не учитывается. Без притоков тепла и диссипации уравнение обладает лишь интегралом энергии. Для двухкомпонентной системы подробно изучаются стационарные состояния, их устойчивость и нелинейное поведение системы вблизи этих состояний. Величина вынуждающей силы определяет число стационарных состояний/одно или три/и их устойчивость. При некоторых значениях силы в окрестности одного из устойчивых стационарных состояний возникает неустойчивый предельный цикл. Те же свойства исследуются и у трехкомпонентной системы как в случае сохранения энергии, так и при наличии внешнего возбуждения и диссипации. Если внешняя сила действует лишь на самую крупномасштабную компоненту, то существует одно устойчивое стационарное состояние. Более сложное поведение система демонстрирует, когда внешнее возбуждение действует и на меньших масштабах. Может появиться устойчивый предельный цикл, а также происходят "катастрофы", т.е. внезапное изменение числа стационарных состояний при незначительной вариации параметра. Обобщать полученные результаты на поведение такой сложной системы, как атмосфера, трудно, если не невозможно. Можно думать, однако, что исследования, подобные проведенному выше, улучшат наше понимание поведения многокомпонентных систем.